Research Article Vol. 36, No. 7 / July 2019 / Journal of the Optical Society of America B E21

Journal of the Optical Society of America B

OPTICAL PHYSICS

Collective lattice resonances in disordered and quasi-random all-dielectric metasurfaces

VADIM I. ZAKOMIRNYI,[1,2,3] SERGEI V. KARPOV,[3,4,5] HANS ÅGREN,[1,2] AND ILIA L. RASSKAZOV[6,*]

[1]Department of Theoretical Chemistry and Biology, School of Engineering Sciences in Chemistry, Biotechnology and Health, Royal Institute of Technology, Stockholm, SE-10691, Sweden
[2]Federal Siberian Research Clinical Centre under FMBA of Russia, Krasnoyarsk, 660037, Russia
[3]Institute of Nanotechnology, Spectroscopy and Quantum Chemistry, Siberian Federal University, Krasnoyarsk 660041, Russia
[4]Siberian State University of Science and Technology, Krasnoyarsk, 660014, Russia
[5]Kirensky Institute of Physics, Federal Research Center KSC SB RAS, Krasnoyarsk, 660036, Russia
[6]The Institute of Optics, University of Rochester, Rochester, New York 14627, USA
*Corresponding author: irasskaz@ur.rochester.edu

Received 18 December 2018; revised 7 March 2019; accepted 13 March 2019; posted 14 March 2019 (Doc. ID 355522); published 16 April 2019

Collective lattice resonances in disordered 2*D* arrays of spherical Si nanoparticles (NPs) have been thoroughly studied within the framework of the coupled dipole approximation. Three types of defects have been analyzed: positional disorder, size disorder, and quasi-random disorder. We show that the positional disorder strongly suppresses either the electric dipole (ED) or the magnetic dipole (MD) coupling, depending on the axis along which the NPs are shifted. Contrarily, size disorder strongly affects only the MD response, while the ED resonance can be almost intact, depending on the lattice configuration. Finally, random removing of NPs from an ordered 2*D* lattice reveals a quite surprising result: hybridization of the ED and MD resonances with lattice modes remains observable even in the case of random removing of up to 84% of the NPs from the ordered array. The reported results could be important for rational design and utilization of metasurfaces, solar cells, and other all-dielectric photonic devices.

https://doi.org/10.1364/JOSAB.36.000E21

1. INTRODUCTION

Strong coupling between lattice modes in arrays of nanoparticles (NPs) and Mie-type oscillations localized within a single NP has attracted significant attention over the last decade. Pioneering theoretical predictions for 1*D* arrays of Ag NPs [1–3] and consequent experimental verification for 2*D* arrays of Au NPs [4–6] have given a momentum to a great number of excellent applications of collective lattice resonances in lasers [7–12], biosensors [13–18], emission enhancement [19–22], and color printing [23–26].

To date, most of the studies have considered diffractive coupling between *electric* dipole (ED) oscillations and Wood–Rayleigh anomalies [27,28] in arrays of classic plasmonic NPs such as Au or Ag. However, quite recently significant attention has been turned to alternative plasmonic materials such as indium-tin-oxide [29], aluminum [30–33], transition metal nitrides [22,34,35], and nickel [36]. The use of these materials makes it possible to tailor a wavelength of collective lattice modes within a wide spectral range, from UV [31] to IR [35], or enable a magneto-optical activity [37,38] that paves the way for a rich variety of novel and promising applications.

In this context, dielectric NPs with both *electric* and *magnetic* dipole (MD) resonances [39] represent a case of specific interest. Arrays of all-dielectric NPs have already found a number of excellent applications in photonics and nanotechnology spanning light-guiding [40–42], metamaterials [43], metasurfaces [44–48], mid-infrared filters [49], and others [50]. However, the coupling between localized oscillations in a single dielectric NP and lattice modes has been addressed only quite recently [51–54], with particular attention to ED and MD coupling [55] and overlapping [56] in 2*D* Si nanodisk arrays.

While various aspects of diffractive behavior of ED and MD resonances in arrays of NPs have been heavily studied in the recent decade [57–60], just a few works have addressed the effects of positional and size disorders [61–63], and only for arrays with pure ED coupling. Quite interesting results have also been reported for lasing [64,65] and solar energy harvesting [62,66–68] in various types of quasi-periodic and aperiodic structures. However, it is a well-known fact that the presence of imperfections in 1*D* chains of NPs [69,70], 2*D* structures [71–76], 3*D* metamaterials [77], and fractal aggregates [78] may lead to various intriguing effects.

In this work, we thoroughly address this problem within the coupled dipole approximation, and study three types of imperfections in 2*D* arrays of Si nanospheres: (i) disorder in positions of Si nanospheres of the same size; (ii) disorder in sizes of Si

nanospheres arranged in an ordered 2*D* lattice; and (iii) quasi-ordered 2*D* arrays of Si nanospheres of the same size. A comprehensive analysis of these scenarios reveals different impact of disorder on ED and MD coupling with lattice modes.

The paper is organized as follows. In Section 2, we provide a theoretical background for the coupled dipole approximation; next, in Section 3 we discuss general features of ED and MD coupling in ordered lattices; then, the impact of positional and size disorder on optical properties of 2*D* lattices of Si NPs, as well as their quasi-random modifications, are discussed in Section 4; Finally, we draw general conclusions in Section 5.

2. COUPLED DIPOLE APPROXIMATION

Consider an array of N spherical NPs embedded in vacuum. Under the incident plane-wave illumination with electric $\mathbf{E}^0$ and magnetic $\mathbf{H}^0$ components, the ith particle located at $\mathbf{r}_i$ acquires electric $\mathbf{d}_i$ and magnetic $\mathbf{m}_i$ dipole moments that are coupled to other dipoles and to an external electromagnetic field via the coupled dipole equations [39,79,80]:

$$\mathbf{d}_i = \alpha_i^e \left(\mathbf{E}_i^0 + \sum_{j\neq i}^{N} \hat{G}_{ij}\mathbf{d}_j - \sqrt{\frac{\mu_0}{\varepsilon_0}} \sum_{j\neq i}^{N} \hat{C}_{ij}\mathbf{m}_j \right), \tag{1a}$$

$$\mathbf{m}_i = \alpha_i^m \left(\mathbf{H}_i^0 + \sum_{j\neq i}^{N} \hat{G}_{ij}\mathbf{m}_j + \sqrt{\frac{\varepsilon_0}{\mu_0}} \sum_{j\neq i}^{N} \hat{C}_{ij}\mathbf{d}_j \right), \tag{1b}$$

where α_i^e and α_i^m are ED and MD polarizabilities of the ith particle, respectively, ε_0 and μ_0 are the dielectric constant and magnetic permeability of vacuum, $\mathbf{E}_i^0 = \mathbf{E}^0(\mathbf{r}_i)$, $\mathbf{H}_i^0 = \mathbf{H}^0(\mathbf{r}_i)$, and

$$\hat{G}_{ij} = A_{ij}\hat{I} + B_{ij}\left(\frac{\mathbf{r}_{ij} \otimes \mathbf{r}_{ij}}{r_{ij}^2}\right), \qquad \hat{C}_{ij} = D_{ij}\frac{\mathbf{r}_{ij}}{r_{ij}}\times, \tag{2}$$

where $\hat{I}$ is a 3×3 unit tensor, $\otimes$ denotes a tensor product, and A_{ij}, B_{ij}, and D_{ij} are defined as follows:

$$A_{ij} = \frac{\exp(ikr_{ij})}{r_{ij}}\left(k^2 - \frac{1}{r_{ij}^2} + \frac{ik}{r_{ij}}\right), \tag{3}$$

$$B_{ij} = \frac{\exp(ikr_{ij})}{r_{ij}}\left(-k^2 + \frac{3}{r_{ij}^2} - \frac{3ik}{r_{ij}}\right), \tag{4}$$

$$D_{ij} = \frac{\exp(ikr_{ij})}{r_{ij}}\left(k^2 + \frac{ik}{r_{ij}}\right), \tag{5}$$

where $r_{ij} = |\mathbf{r}_{ij}| = |\mathbf{r}_i - \mathbf{r}_j|$ is the center-to-center distance between the ith and jth particles, $k = 2\pi/\lambda$ is a wavenumber, and λ is a wavelength of external illumination.

ED and MD polarizabilities are explicitly defined as [81]

$$\alpha_i^e = \frac{3i}{2k^3}\frac{n\psi_1(nkR_i)\psi_1'(kR_i) - \psi_1(kR_i)\psi_1'(nkR_i)}{n\psi_1(nkR_i)\xi_1'(kR_i) - \xi_1(kR_i)\psi_1'(nkR_i)}, \tag{6}$$

$$\alpha_i^m = \frac{3i}{2k^3}\frac{\psi_1(nkR_i)\psi_1'(kR_i) - n\psi_1(kR_i)\psi_1'(nkR_i)}{\psi_1(nkR_i)\xi_1'(kR_i) - n\xi_1(kR_i)\psi_1'(nkR_i)}, \tag{7}$$

where n is the refractive index of the NP material, R_i is the radius of the ith particle, $\psi_1(x)$ and $\xi_1(x)$ are Riccati–Bessel functions, and prime denotes the derivation with respect to the argument in parentheses.

The electric $\mathbf{d}_i$ and magnetic $\mathbf{m}_i$ dipoles induced on each NP can be found from the solution of Eq. (1). In this work, we describe the optical response of the arrays of NPs with the extinction efficiency

$$Q_e = \frac{4k}{I_0 N\langle R\rangle^2}\,\mathrm{Im}\sum_{i=1}^{N}\left(\mathbf{d}_i\cdot\mathbf{E}_i^{0*} + \frac{\mu_0}{\varepsilon_0}\mathbf{m}_i\cdot\mathbf{H}_j^{0*}\right), \tag{8}$$

where I_0 is the intensity of the incident field, and the asterisk denotes a complex conjugate. Note that in the general case of polydisperse array with $R_i \neq R$, the mean radius $\langle R\rangle = \sum_{i=1}^{N} R_i/N$ is used to define Q_e.

The coupled dipole approximation quite accurately describes optical properties of arrays from relatively small Si NPs. Full-wave simulations [82] show that ED and MD are predominant in arrays of Si NPs with $R = 65$ nm, and high-order electric and magnetic field oscillations can be ignored in this case, though higher-order multipoles in all-dielectric NPs are pronounced, for example, in large [83–85] and nonspherical [86] single Si NPs, or closely packed arrays of Si NPs [40].

3. ORDERED ARRAYS

We start with the optical properties of a single Si nanosphere. Though it has been widely discussed in the literature, for instance, in Ref. [39], we plot these results for the reader's convenience. Figure 1(a) shows the refractive index of Si used in calculations [87], while Fig. 1(b) shows the extinction efficiency Q_e for a single Si nanosphere of various radii R. For a single sphere, and only in this case, we calculate Q_e, taking into account high-order harmonics [81] required for the convergence of the electromagnetic light scattering problem [88]. It can be seen from Fig. 1(b) that indeed, for given sizes, Si nanospheres have distinct and predominant ED and MD resonances in the visible wavelength range. In what follows, we consider arrays from Si nanospheres with $R = 65$ nm radius. However, in the special case of a size disorder, all possible radii of NPs will fall into the range shown in Fig. 1(b), i.e., $50\ \text{nm} \leq R_i \leq 80$ nm. Therefore, the coupled dipole approximation can be used with strong confidence.

Next, it is insightful to discuss optical properties of *ordered* Si nanostructures. Figures 2(a) and 2(b) show two different types of lattices that have been studied in this work: (i) with fixed period along the x axis, h_x, and varying period along

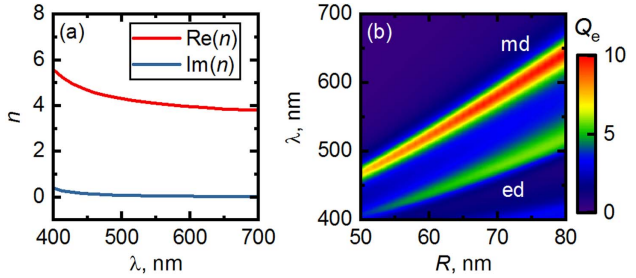

Fig. 1. (a) Refractive index n of Si from Ref. [87]; (b) extinction spectra for a single Si NP of various radii R, taking into account high-order multipoles. Spectral positions of ED and MD resonances are denoted as "ed" and "md," respectively.

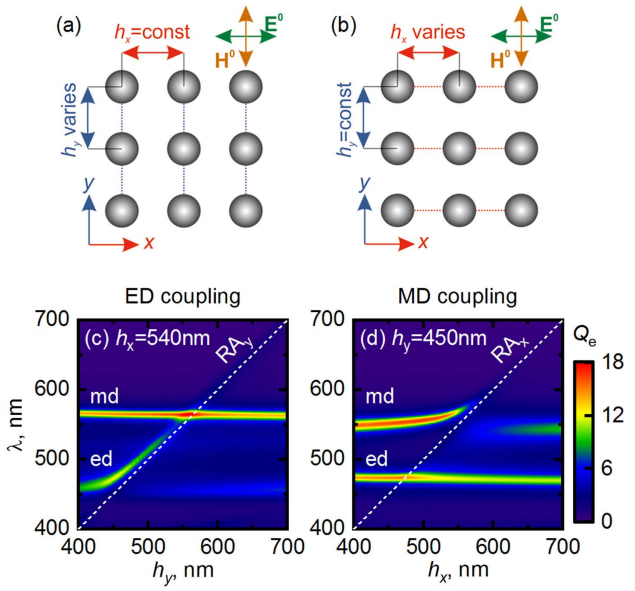

Fig. 2. (a) and (b) Schematic representation, and (c) and (d) extinction spectra Q_e of ordered 2*D* lattices from $N = 20 \times 20$ Si NPs with $R = 65$ nm. Two configurations are considered: (left) fixed $h_x = 540$ nm and varying h_y, and (right) fixed $h_y = 450$ nm and varying h_x. Spectral positions of ED and MD resonances are denoted as "ed" and "md," respectively. Dashed RA_x and RA_y lines denote Rayleigh anomalies $\lambda = h_x$ and $\lambda = h_y$, correspondingly.

the *y* axis, h_y, and (ii) with fixed h_y and varying h_x. Such variations of interparticle distances make it possible to get ED or MD coupling with lattice modes [55]. In both cases, the incident electric $\mathbf{E}^0$ and magnetic $\mathbf{H}^0$ fields are aligned along the *x* and *y* axes, correspondingly. Lattices from $N = 20 \times 20$ Si NPs have been considered.

In the first case, as is clearly seen from Fig. 2(c), ED strongly couples to lattice modes, which leads to the emergence of quite sharp collective lattice resonances. The position of the MD resonance slightly shifts to shorter wavelengths for large h_y. Note that Q_e for MD increases near the Rayleigh anomaly $\lambda = h_y$. In the second case, according to Fig. 2(d), the same strong coupling with lattice modes occurs for MD, while the position of ED gradually shifts to shorter wavelengths, and the corresponding Q_e decreases with increasing h_x. Thus, the coupling occurs for the incident field (electric or magnetic) perpendicular to the axis along which the interparticle distance is changed. In other words, for the particular case considered in this work, EDs ($\mathbf{E}^0$ is parallel to *x* axis) couple to RA_y, and, vice versa, MDs ($\mathbf{H}^0$ is parallel to *y* axis) couple to RA_x.

4. DISORDERED ARRAYS

A. Types of Disorder

According to Eq. (1), two types of disorder can be distinguished [69]: (i) off-diagonal and (ii) diagonal. These types affect either off-diagonal or diagonal elements of the interaction matrix in Eq. (1), respectively. The first type of disorder affects only tensors $\hat{G}_{ij}$ and $\hat{C}_{ij}$, which are the functions of the NPs' positions, while the second type of disorder affects only $\alpha_i^{e,m}$, which are the functions of NPs' shape and size.

As was shown for ordered arrays of NPs in Fig. 2, two types of coupling can be distinguished. For fixed illumination, optical response of lattices strongly depends on variations of either h_x and h_y. Thus, to get more insight, we introduce the off-diagonal disorder in the following manner. We study positional disorder along the *x* axis, keeping *y* coordinates constant, and vice versa, as shown in Figs. 3(a) and 3(b), respectively. We will refer to these two types of positional disorder as *x* disorder and *y* disorder, correspondingly. For both cases, we introduce deviations $\sigma_{x,y}$, which characterize a degree of disorder. For each *i*th particle with initial (x_i, y_i) coordinates, we randomly set new coordinates as (x_i^{dis}, y_i) for *x* disorder and (x_i, y_i^{dis}) for *y* disorder within the following limits:

$$x_i - \sigma_x \le x_i^{\text{dis}} \le x_i + \sigma_x, \quad \text{and} \quad y_i - \sigma_y \le y_i^{\text{dis}} \le y_i + \sigma_y. \tag{9}$$

Both x_i^{dis} and y_i^{dis} are randomly generated using a uniform distribution for each *i*th NP and for each lattice with given (h_x, h_y). Thus, the effects of positional disorder are uncorrelated.

The schematics of the lattice with diagonal (size) disorder is shown in Fig. 3(c). In this case, we keep original coordinates of each NP, and randomly change the radius R_i of each *i*th NP within the following limits using a uniform distribution:

$$R_i - \sigma_R \le R_i^{\text{dis}} \le R_i + \sigma_R. \tag{10}$$

Again, as in the case of off-diagonal disorder, R_i^{dis} is introduced randomly for each NP and for each lattice configuration, which provides uncorrelated results.

Finally, Fig. 3(d) shows a special combination of diagonal and off-diagonal disorders, which attracts specific interest [64,65]. It is a well-known fact that the coupling between a single NP resonance and lattice modes strongly depends on the number of NPs in the array [89,90]. However, periodic lattices

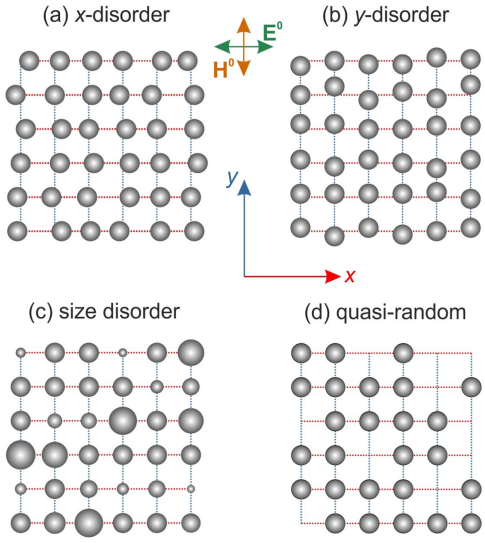

Fig. 3. Schematic representation of different types of disorder considered in this work: (a) *x* disorder, (b) *y* disorder, (c) size disorder, and (d) quasi-random array.

of strictly arranged NPs are usually considered to study this finite-sized effect. In our work, we fix the initial coordinates and the sizes of NPs, and randomly remove NPs from the lattice, keeping other NPs untouched. This type of imperfection is somewhat similar to vacancies in crystal structures. In what follows, we will refer to lattices shown in Fig. 3(d) as quasi-random arrays.

We emphasize that each lattice configuration for each type of disorder with given σ_x, σ_y, and σ_R, or number of NPs removed from the lattice in the case of quasi-random arrays, has been simulated only once, without computing ensemble averages. A reasonable closeness to statistical average has been granted by simulating a large enough number of NPs.

B. Off-Diagonal (Positional) Disorder

Figures 4 and 5 show extinction spectra for arrays of NPs with different degrees of x and y disorders. It can be seen that these two types of positional disorder affect the optical properties of NPs in a different way, depending on the coupling regime.

As might be expected from the analysis of Fig. 2(d), the x disorder significantly affects MD, since the latter strongly couples to the Rayleigh anomaly RA_x. Clearly, from Fig. 4, one may observe a slight suppression of the MD with the increasing of the degree of disorder, σ_x, both for ED and MD coupling scenarios. It also has to be noted that the coupling of MD and RA_x remains observable even for sufficiently large σ_x in Fig. 4(f), where MD is suppressed. The ED remains almost the same for each case shown in Fig. 4.

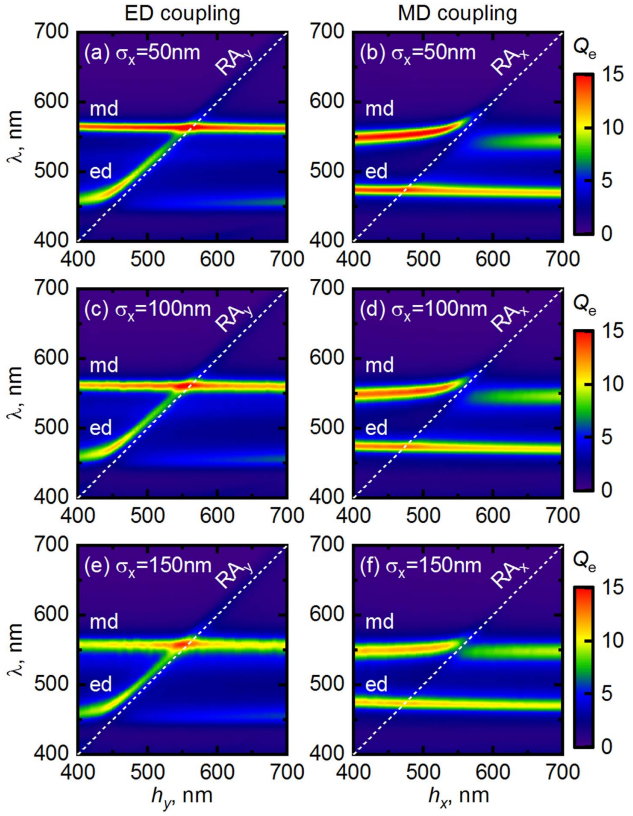

Fig. 4. Extinction spectra Q_e for the same $2D$ lattices as in Figs. 2(c) and 2(d), but for various degrees of positional disorder σ_x along the x axis, as shown in Fig. 3(a).

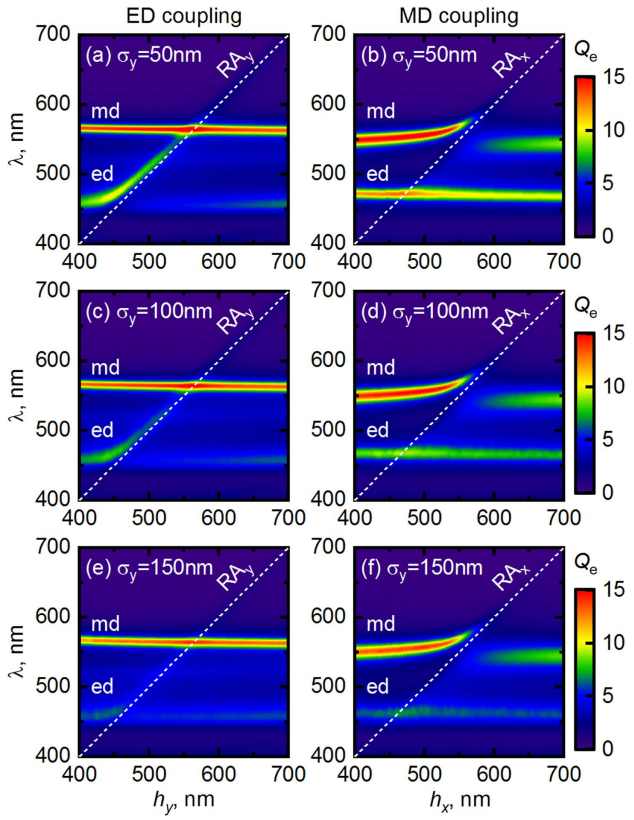

Fig. 5. Same as in Fig. 4, but for various degrees of positional disorder σ_y along the y axis, as shown in Fig. 3(b).

Figure 5 shows an expected trend: since ED couples to RA_y, the y disorder affects only the former, keeping MD almost the same for various σ_y. However, Figs. 5(e) and 5(f) show almost total suppression of ED for $\sigma_y = 150$ nm, while in the case of strong x disorder shown in Figs. 4(e) and 4(f), MD is quite pronounced.

Finally, Fig. 6 shows a detailed comparison of the extinction spectra for arrays with ED or MD couplings. Indeed, the x disorder strongly suppresses the MD, while the y disorder suppresses the ED resonance. Since the ED is generally weaker than the MD, the former almost completely disappears for high degrees of y disorder. For completeness, Figs. 6(g) and 6(h) show spectra for arrays with xy disorder, which has been introduced in the same way as the x and y disorders, but with simultaneous randomization of both x_i and y_i coordinates of each NP. It can be seen that, in general, such a combined disorder yields a superposition of both x and y disorders suppresses both ED and MD resonances.

C. Diagonal (Size) Disorder

Figure 7 shows extinction spectra for arrays with various degrees of size disorder, σ_R. It is clearly seen that random variations of NP sizes strongly suppress both ED and MD resonances. However, MD remains observable only for $\sigma_R = 5$ nm, while for larger σ_R, it almost completely disappears. Contrarily, the ED resonance is preserved in all cases, and, of note, EDs strongly couple with Rayleigh anomalies,

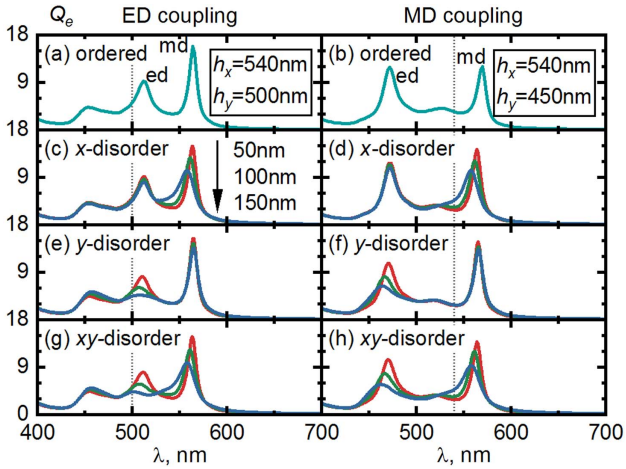

Fig. 6. Extinction spectra Q_e of NPs arrays with ED coupling (left), and MD coupling (right) for various degrees of positional disorder (c) and (d) σ_x, (e) and (f) σ_y, and (g) and (h) σ_{xy}. Corresponding values of h_x and h_y are shown in legends. Dashed vertical lines denote positions of Rayleigh anomalies RA_y at $\lambda = 500$ nm (left), and RA_x at $\lambda = 540$ nm (right).

RA_y, even for high degrees of diagonal disorder, as shown in Fig. 7(e). This effect might be explained by the different behavior of polarizabilities α_i^e and α_i^m [39], which yield a different impact of size disorder on ED and MD resonances.

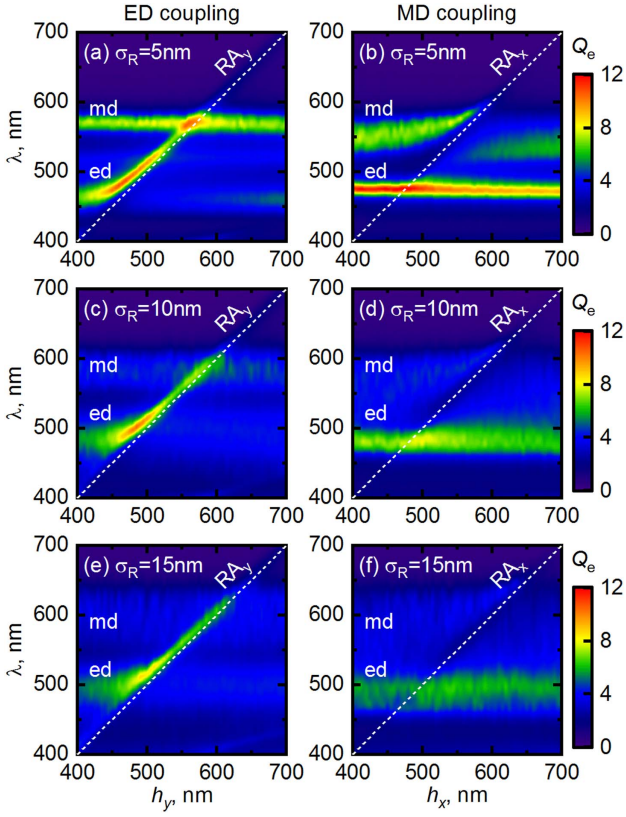

Fig. 7. Extinction spectra Q_e for the same 2D lattices as in Figs. 2(c) and 2(d), but for various degrees of size disorder σ_R, as shown in Fig. 3(c).

To get a deeper insight, we plot Q_e for arrays with fixed h_x and h_y, as shown in Fig. 8. Indeed, Figs. 8(c), 8(e), and 8(g) show that size disorder has a surprisingly weak effect on the ED resonance of arrays with strong ED coupling. It can be seen from Fig. 8(g) that maximum Q_e for the ED resonance drops by no more than 10% for $\sigma_R = 15$ nm compared to the ordered array shown in Fig. 8(a). For arrays with MD coupling, Q_e for ED resonance drops more strongly, by a factor of 2 for $\sigma_R = 15$ nm, as shown in Fig. 8(h). As for the MD resonance, in both the ED and MD coupling cases, the extinction efficiency for MD sharply drops for $\sigma_R = 5$ nm. For larger σ_R, the MD resonance becomes almost indistinguishable.

D. Quasi-Random Arrays

From the previous discussion of diagonal and off-diagonal types of disorder, we can conclude that a simultaneous implementation of positional and size disorders should likely result in the superposition of the effects shown in Figs. 4, 5, and 7. Thus, we do not consider arrays of randomly located NPs of different size. Instead, we introduce a specific combination of positional and size disorders, as shown in Fig. 3(d). These quasi-random arrays are fundamentally different from those shown in Figs. 3(a)–3(c), since random elements of the interaction matrix in Eq. (1) are strictly set to zero in the case of quasi-random arrays, while in previously considered scenarios, off-diagonal or diagonal elements have acquired random deviations according to σ_x, σ_y, or σ_R.

Here, we consider NPs with the same size, $R = 65$ nm, but increase their number to $N = 30 \times 30$ (while previously discussed arrays had $N = 20 \times 20$ NPs). Next, we randomly remove 171, 459, or 756 NPs, leaving the rest 81%, 49%, or 16% of NPs untouched, respectively. We note that the consideration of larger arrays is preferable for this type of disorder, since coupling effects may be totally suppressed in arrays from the small number of NPs left in the lattice [89]. However, in the smallest array considered here, we keep 144 quasi-randomly

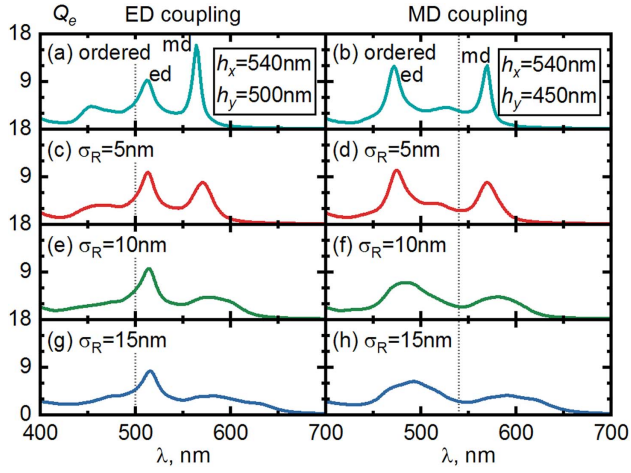

Fig. 8. Extinction spectra Q_e of NP arrays with ED coupling (left), and MD coupling (right) for various degrees of size disorder σ_R. Corresponding values of h_x and h_y are shown in legends. Dashed vertical lines denote positions of Rayleigh anomalies RA_y at $\lambda = 500$ nm (left), and RA_x at $\lambda = 540$ nm (right).

located NPs, which is sufficient for the emergence of coupling effects.

Intuitively, one could expect the suppression of ED and MD couplings with the increasing number of NPs removed from the ordered array. Indeed, Fig. 9 confirms such an expectation. However, it can be seen that lattices that contain 81% of the initial NPs have almost the same optical properties as the original periodic arrays. Moreover, Figs. 9(e)–9(f) show that ED and MD are coupled to Rayleigh anomalies (though quite weakly) in the arrays with only 16% NPs left, and extinction spectra of such arrays tend to become closer to Q_e of a single NP.

For comparison, Fig. 10 shows spectra of ordered arrays [as in Figs. 2(a) and 2(b)] from exactly the same number of NPs as in quasi-random arrays, i.e., 27 × 27, 21 × 21, and 12 × 12, and with the same h_x and h_y. It can be seen from Figs. 10(c) and 10(d) that Q_e of the quasi-random array from 729 NPs is also almost the same as Q_e for the periodic 27 × 27 array. Moreover, even with the increasing number of NPs removed from the array, Q_e of the quasi-random lattices is quite close to that for the strictly ordered arrays with the same number of NPs. However, in the most extreme cases of quasi-random arrays shown in Figs. 10(g) and 10(h), the collective ED resonances are almost suppressed, while the MD coupling remains observable, although the corresponding peak of MD resonance is blue-shifted compared with the ordered arrays.

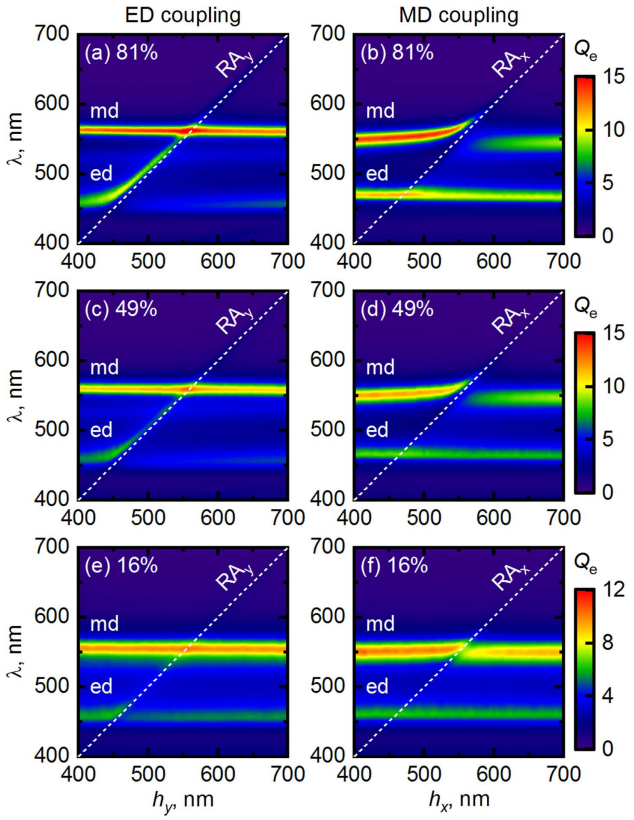

Fig. 9. Extinction spectra Q_e for quasi-random 2*D* lattices, as shown in Fig. 3(d), for different numbers of NPs. (a) and (b) 81% = 729, (c) and (d) 49% = 441, and (e) and (f) 16% = 144 kept untouched in $N = 30 \times 30$ arrays of NPs with $R = 65$ nm. Note the different color scale in the last row, (e) and (f).

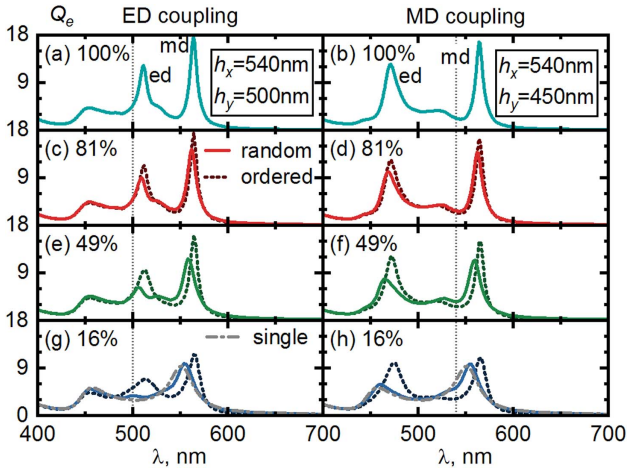

Fig. 10. Extinction spectra Q_e of NPs arrays with ED coupling (left), and MD coupling (right) for (a) and (b) $N = 30 \times 30$ array, and for its various quasi-random modifications (solid lines); (c) and (d) 81% = 729, (e) and (f) 49% = 441; and (g) and (h) 16% = 144 (NPs kept untouched). For comparison, Q_e of strictly periodic (dashed lines) arrays of the same number of NPs are shown; (c) and (d) $N = 27 \times 27 = 729$; (e) and (f) $N = 21 \times 21 = 441$; and (g) and (h) $N = 12 \times 12 = 144$; gray dashed-dotted lines show Q_e of a single Si NP with $R = 65$ nm. Corresponding values of h_x and h_y are shown in legends. Dashed vertical lines denote positions of Rayleigh anomalies RA_y at $\lambda = 500$ nm (left), and RA_x at $\lambda = 540$ nm (right).

5. CONCLUSION

We have theoretically analyzed the impact of various types of imperfections on the optical response of 2*D* arrays of spherical Si NPs. ED and MD resonances are dominant in Si nanospheres in the considered range 50 nm ≤ R ≤ 80 nm; thus, we have used the coupled dipole approximation, which adequately describes electromagnetic properties of Si NP arrays [82].

We first have shown the existence of two types of collective resonances in 2*D* arrays emerging from the strong coupling of either ED or MD resonances of a single NP with lattice modes (Rayleigh anomalies) of the 2*D* array. Such a coupling occurs when the corresponding component of the incident field (electric or magnetic) is orthogonal to the varied period (h_y or h_x) of the lattice, while the other period (h_x or h_y) is constant [55].

Second, we have shown that electric or magnetic responses are affected by the positional disorder only when NPs are shifted along the axis that is orthogonal to the corresponding component of incident electromagnetic illumination. In our case, for $\mathbf{E}^0 \| x$ and $\mathbf{H}^0 \| y$, ED and MD resonances are strongly suppressed only for y or x disorders, respectively. Obviously, both resonances are affected when NPs are shifted along the x and y axes simultaneously.

Next, we have demonstrated that the collective MD response almost completely vanishes in the case of diagonal (size) disorder with $\sigma_R > 5$ nm. However, the electric counterpart remains quite stable, especially in the case of strong collective coupling between the ED resonance and lattice modes, even for highly polydisperse arrays with $\sigma_R = 15$ nm.

Finally, we have considered quasi-random arrays as a special combination of off-diagonal and diagonal disorders. Instead of simultaneously shifting the NPs and changing their sizes, we have randomly removed NPs from the lattice, keeping other NPs at original points with original sizes. Surprisingly, arrays with only 16% of NPs left in the lattice exhibit both electric and magnetic collective resonances. However, the extinction spectra of such arrays tend to be similar to spectra of a single NP.

The reported results provide a comprehensive analysis and a fundamental understanding of the impact that disorder has on collective resonances in $2D$ arrays of all-dielectric NPs. While we have considered spherical Si NPs embedded in vacuum, one could expect similar trends for all-dielectric arrays of NPs of other shapes or materials [91] as long as high-order multipoles can be neglected. Thus, we believe that the reported results may pave the way for future applications in all-dielectric nanophotonics.

Funding. Russian Foundation for Basic Research (RFBR) (18-42-240013); Russian Science Foundation (RSF) (18-13-00363); Siberian Federal University (SibFU) (3.8896.2017).

Acknowledgment. The reported study was funded by Russian Foundation for Basic Research, Government of Krasnoyarsk Territory, Krasnoyarsk Regional Fund of Science, the research project No 18-42-240013; the State contract with Siberian Federal University for scientific research in 2017–2019 (Grant No.3.8896.2017). H. A. and V. Z. acknowledge the support of the Russian Science Foundation (Project No.18-13-00363) (numerical calculations of spectral properties of planar dielectric nanostructures).

REFERENCES

1. S. Zou and G. C. Schatz, "Narrow plasmonic/photonic extinction and scattering line shapes for one and two dimensional silver nanoparticle arrays," J. Chem. Phys. **121**, 12606–12612 (2004).
2. S. Zou, N. Janel, and G. C. Schatz, "Silver nanoparticle array structures that produce remarkably narrow plasmon lineshapes," J. Chem. Phys. **120**, 10871–10875 (2004).
3. V. A. Markel, "Divergence of dipole sums and the nature of non-Lorentzian exponentially narrow resonances in one-dimensional periodic arrays of nanospheres," J. Phys. B **38**, L115–L121 (2005).
4. B. Auguié and W. L. Barnes, "Collective resonances in gold nanoparticle arrays," Phys. Rev. Lett. **101**, 143902 (2008).
5. Y. Chu, E. Schonbrun, T. Yang, and K. B. Crozier, "Experimental observation of narrow surface plasmon resonances in gold nanoparticle arrays," Appl. Phys. Lett. **93**, 181108 (2008).
6. V. G. Kravets, F. Schedin, and A. N. Grigorenko, "Extremely narrow plasmon resonances based on diffraction coupling of localized plasmons in arrays of metallic nanoparticles," Phys. Rev. Lett. **101**, 087403 (2008).
7. F. van Beijnum, P. J. van Veldhoven, E. J. Geluk, M. J. A. de Dood, G. W't Hooft, and M. P. van Exter, "Surface plasmon lasing observed in metal hole arrays," Phys. Rev. Lett. **110**, 206802 (2013).
8. W. Zhou, M. Dridi, J. Y. Suh, C. H. Kim, D. T. Co, M. R. Wasielewski, G. C. Schatz, and T. W. Odom, "Lasing action in strongly coupled plasmonic nanocavity arrays," Nat. Nanotechnol. **8**, 506–511 (2013).
9. M. Dridi and G. C. Schatz, "Model for describing plasmon-enhanced lasers that combines rate equations with finite-difference time-domain," J. Opt. Soc. Am. B **30**, 2791–2797 (2013).
10. A. H. Schokker and A. F. Koenderink, "Lasing at the band edges of plasmonic lattices," Phys. Rev. B **90**, 155452 (2014).
11. D. Wang, W. Wang, M. P. Knudson, G. C. Schatz, and T. W. Odom, "Structural engineering in plasmon nanolasers," Chem. Rev. **118**, 2865–2881 (2018).
12. A. H. Schokker, F. van Riggelen, Y. Hadad, A. Alù, and A. F. Koenderink, "Systematic study of the hybrid plasmonic-photonic band structure underlying lasing action of diffractive plasmon particle lattices," Phys. Rev. B **95**, 085409 (2017).
13. R. Adato, A. A. Yanik, J. J. Amsden, D. L. Kaplan, F. G. Omenetto, M. K. Hong, S. Erramilli, and H. Altug, "Ultra-sensitive vibrational spectroscopy of protein monolayers with plasmonic nanoantenna arrays," Proc. Natl. Acad. Sci. USA **106**, 19227–19232 (2009).
14. V. G. Kravets, F. Schedin, A. V. Kabashin, and A. N. Grigorenko, "Sensitivity of collective plasmon modes of gold nanoresonators to local environment," Opt. Lett. **35**, 956–958 (2010).
15. R. Adato and H. Altug, "In-situ ultra-sensitive infrared absorption spectroscopy of biomolecule interactions in real time with plasmonic nanoantennas," Nat. Commun. **4**, 2154 (2013).
16. B. D. Thackray, V. G. Kravets, F. Schedin, G. Auton, P. A. Thomas, and A. N. Grigorenko, "Narrow collective plasmon resonances in nanostructure arrays observed at normal light incidence for simplified sensing in asymmetric air and water environments," ACS Photon. **1**, 1116–1126 (2014).
17. A. Danilov, G. Tselikov, F. Wu, V. G. Kravets, I. Ozerov, F. Bedu, A. N. Grigorenko, and A. V. Kabashin, "Ultra-narrow surface lattice resonances in plasmonic metamaterial arrays for biosensing applications," Biosens. Bioelectron. **104**, 102–112 (2018).
18. R. R. Gutha, S. M. Sadeghi, A. Hatef, C. Sharp, and Y. Lin, "Ultrahigh refractive index sensitivity via lattice-induced meta-dipole modes in flat metallic nanoantenna arrays," Appl. Phys. Lett. **112**, 223102 (2018).
19. G. Vecchi, V. Giannini, and J. Gómez Rivas, "Shaping the fluorescent emission by lattice resonances in plasmonic crystals of nanoantennas," Phys. Rev. Lett. **102**, 146807 (2009).
20. M. Ramezani, G. Lozano, M. A. Verschuuren, and J. Gómez-Rivas, "Modified emission of extended light emitting layers by selective coupling to collective lattice resonances," Phys. Rev. B **94**, 125406 (2016).
21. F. Laux, N. Bonod, and D. Gérard, "Single emitter fluorescence enhancement with surface lattice resonances," J. Phys. Chem. C **121**, 13280–13289 (2017).
22. R. Kamakura, S. Murai, K. Fujita, and K. Tanaka, "Enhanced photoluminescence from organic dyes coupled to periodic array of zirconium nitride nanoparticles," ACS Photon. **5**, 3057–3063 (2018).
23. A. S. Roberts, A. Pors, O. Albrektsen, and S. I. Bozhevolnyi, "Subwavelength plasmonic color printing protected for ambient use," Nano Lett. **14**, 783–787 (2014).
24. X. Duan, S. Kamin, and N. Liu, "Dynamic plasmonic colour display," Nat. Commun. **8**, 14606 (2017).
25. H. Wang, X. Wang, C. Yan, H. Zhao, J. Zhang, C. Santschi, and O. J. F. Martin, "Full color generation using silver tandem nanodisks," ACS Nano **11**, 4419–4427 (2017).
26. H. Bertin, Y. Brûlé, G. Magno, T. Lopez, P. Gogol, L. Pradere, B. Gralak, D. Barat, G. Demésy, and B. Dagens, "Correlated disordered plasmonic nanostructures arrays for augmented reality," ACS Photon. **5**, 2661–2668 (2018).
27. R. W. Wood, "On a remarkable case of uneven distribution of light in a diffraction grating spectrum," Proc. Phys. Soc. London **18**, 269–275 (1902).
28. Lord Rayleigh, "On the dynamical theory of gratings," Proc. R. Soc. London A **79**, 399–416 (1907).
29. S.-Q. Li, P. Guo, D. B. Buchholz, W. Zhou, Y. Hua, T. W. Odom, J. B. Ketterson, L. E. Ocola, K. Sakoda, and R. P. H. Chang, "Plasmonic-photonic mode coupling in indium-tin-oxide nanorod arrays," ACS Photon. **1**, 163–172 (2014).
30. A. Yang, A. J. Hryn, M. R. Bourgeois, W.-K. Lee, J. Hu, G. C. Schatz, and T. W. Odom, "Programmable and reversible plasmon mode engineering," Proc. Natl. Acad. Sci. USA **113**, 14201–14206 (2016).
31. D. Khlopin, F. Laux, W. P. Wardley, J. Martin, G. A. Wurtz, J. Plain, N. Bonod, A. V. Zayats, W. Dickson, and D. Gérard, "Lattice modes and plasmonic linewidth engineering in gold and aluminum nanoparticle arrays," J. Opt. Soc. Am. B **34**, 691–700 (2017).

32. M. L. Tseng, J. Yang, M. Semmlinger, C. Zhang, P. Nordlander, and N. J. Halas, "Two-dimensional active tuning of an aluminum plasmonic array for full-spectrum response," Nano Lett. **17**, 6034–6039 (2017).
33. Y. Kawachiya, S. Murai, M. Saito, H. Sakamoto, K. Fujita, and K. Tanaka, "Collective plasmonic modes excited in Al nanocylinder arrays in the UV spectral region," Opt. Express **26**, 5970–5982 (2018).
34. R. Kamakura, S. Murai, S. Ishii, T. Nagao, K. Fujita, and K. Tanaka, "Plasmonic-photonic hybrid modes excited on a titanium nitride nanoparticle array in the visible region," ACS Photon. **4**, 815–822 (2017).
35. V. I. Zakomirnyi, I. L. Rasskazov, V. S. Gerasimov, A. E. Ershov, S. P. Polyutov, and S. V. Karpov, "Refractory titanium nitride two-dimensional structures with extremely narrow surface lattice resonances at telecommunication wavelengths," Appl. Phys. Lett. **111**, 123107 (2017).
36. M. Kataja, T. K. Hakala, A. Julku, M. J. Huttunen, S. van Dijken, and P. Törmä, "Surface lattice resonances and magneto-optical response in magnetic nanoparticle arrays," Nat. Commun. **6**, 7072 (2015).
37. M. Kataja, S. Pourjamal, N. Maccaferri, P. Vavassori, T. K. Hakala, M. J. Huttunen, P. Törmä, and S. van Dijken, "Hybrid plasmonic lattices with tunable magneto-optical activity," Opt. Express **24**, 3652–3662 (2016).
38. A. Christofi, Y. Kawaguchi, A. Alù, and A. B. Khanikaev, "Giant enhancement of Faraday rotation due to electromagnetically induced transparency in all-dielectric magneto-optical metasurfaces," Opt. Lett. **43**, 1838–1841 (2018).
39. A. B. Evlyukhin, C. Reinhardt, A. Seidel, B. S. Luk'Yanchuk, and B. N. Chichkov, "Optical response features of Si-nanoparticle arrays," Phys. Rev. B **82**, 1–12 (2010).
40. R. S. Savelev, A. P. Slobozhanyuk, A. E. Miroshnichenko, Y. S. Kivshar, and P. A. Belov, "Subwavelength waveguides composed of dielectric nanoparticles," Phys. Rev. B **89**, 035435 (2014).
41. E. N. Bulgakov and D. N. Maksimov, "Light guiding above the light line in arrays of dielectric nanospheres," Opt. Lett. **41**, 3888–3891 (2016).
42. R. M. Bakker, Y. F. Yu, R. Paniagua-Domínguez, B. Luk'yanchuk, and A. I. Kuznetsov, "Resonant light guiding along a chain of silicon nanoparticles," Nano Lett. **17**, 3458–3464 (2017).
43. Q. Zhao, J. Zhou, F. Zhang, and D. Lippens, "Mie resonance-based dielectric metamaterials," Mater. Today **12**(12), 60–69 (2009).
44. A. Arbabi, Y. Horie, M. Bagheri, and A. Faraon, "Dielectric metasurfaces for complete control of phase and polarization with subwavelength spatial resolution and high transmission," Nat. Nanotechnol. **10**, 937–943 (2015).
45. M. I. Shalaev, J. Sun, A. Tsukernik, A. Pandey, K. Nikolskiy, and N. M. Litchinitser, "High-efficiency all-dielectric metasurfaces for ultracompact beam manipulation in transmission mode," Nano Lett. **15**, 6261–6266 (2015).
46. V. E. Babicheva, M. I. Petrov, K. V. Baryshnikova, and P. A. Belov, "Reflection compensation mediated by electric and magnetic resonances of all-dielectric metasurfaces [Invited]," J. Opt. Soc. Am. B **34**, D18–D28 (2017).
47. M. G. Barsukova, A. S. Shorokhov, A. I. Musorin, D. N. Neshev, Y. S. Kivshar, and A. A. Fedyanin, "Magneto-optical response enhanced by Mie resonances in nanoantennas," ACS Photon. **4**, 2390–2395 (2017).
48. V. E. Babicheva and A. B. Evlyukhin, "Resonant suppression of light transmission in high-refractive-index nanoparticle metasurfaces," Opt. Lett. **43**, 5186–5189 (2018).
49. F. Shen, Q. Kang, J. Wang, K. Guo, Q. Zhou, and Z. Guo, "Dielectric metasurface-based high-efficiency mid-infrared optical filter," Nanomaterials **8**, 938 (2018).
50. S. Kruk and Y. Kivshar, "Functional meta-optics and nanophotonics governed by Mie resonances," ACS Photon. **4**, 2638–2649 (2017).
51. S. Tsoi, F. J. Bezares, A. Giles, J. P. Long, O. J. Glembocki, J. D. Caldwell, and J. Owrutsky, "Experimental demonstration of the optical lattice resonance in arrays of Si nanoresonators," Appl. Phys. Lett. **108**, 111101 (2016).
52. L. Zhang, C. Ge, K. Zhang, C. Tian, X. Fang, W. Zhai, L. Tao, Y. Li, and G. Ran, "Lattice plasmons in dielectric nanoparticle arrays arranged on metal film," J. Opt. **18**, 125002 (2016).
53. C.-Y. Yang, J.-H. Yang, Z.-Y. Yang, Z.-X. Zhou, M.-G. Sun, V. E. Babicheva, and K.-P. Chen, "Nonradiating silicon nanoantenna metasurfaces as narrowband absorbers," ACS Photon. **5**, 2596–2601 (2018).
54. D. Tzarouchis and A. Sihvola, "Light scattering by a dielectric sphere: perspectives on the Mie resonances," Appl. Sci. **8**, 184 (2018).
55. J. Li, N. Verellen, and P. Van Dorpe, "Engineering electric and magnetic dipole coupling in arrays of dielectric nanoparticles," J. Appl. Phys. **123**, 083101 (2018).
56. V. E. Babicheva and J. V. Moloney, "Lattice effect influence on the electric and magnetic dipole resonance overlap in a disk array," Nanophotonics **7**, 1663–1668 (2018).
57. M. B. Ross, C. A. Mirkin, and G. C. Schatz, "Optical properties of one-, two-, and three-dimensional arrays of plasmonic nanostructures," J. Phys. Chem. C **120**, 816–830 (2016).
58. B. B. Rajeeva, L. Lin, and Y. Zheng, "Design and applications of lattice plasmon resonances," Nano Res. **11**, 4423–4440 (2018).
59. W. Wang, M. Ramezani, A. I. Väkeväinen, P. Törmä, J. G. Rivas, and T. W. Odom, "The rich photonic world of plasmonic nanoparticle arrays," Mater. Today **21**(3), 303–314 (2018).
60. V. G. Kravets, A. V. Kabashin, W. L. Barnes, and A. N. Grigorenko, "Plasmonic surface lattice resonances: a review of properties and applications," Chem. Rev. **118**, 5912–5951 (2018).
61. B. Auguié and W. L. Barnes, "Diffractive coupling in gold nanoparticle arrays and the effect of disorder," Opt. Lett. **34**, 401–403 (2009).
62. Y. Nishijima, L. Rosa, and S. Juodkazis, "Surface plasmon resonances in periodic and random patterns of gold nano-disks for broadband light harvesting," Opt. Express **20**, 11466–11477 (2012).
63. M. B. Ross, J. C. Ku, M. G. Blaber, C. A. Mirkin, and G. C. Schatz, "Defect tolerance and the effect of structural inhomogeneity in plasmonic DNA-nanoparticle superlattices," Proc. Natl. Acad. Sci. USA **112**, 10292–10297 (2015).
64. A. H. Schokker and A. F. Koenderink, "Statistics of randomized plasmonic lattice lasers," ACS Photon. **2**, 1289–1297 (2015).
65. A. H. Schokker and A. F. Koenderink, "Lasing in quasi-periodic and aperiodic plasmon lattices," Optica **3**, 686–693 (2016).
66. F. Pratesi, M. Burresi, F. Riboli, K. Vynck, and D. S. Wiersma, "Disordered photonic structures for light harvesting in solar cells," Opt. Express **21**, A460–A468 (2013).
67. Y. J. Donie, M. Smeets, A. Egel, F. Lentz, J. B. Preinfalk, A. Mertens, V. Smirnov, U. Lemmer, K. Bittkau, and G. Gomard, "Light trapping in thin film silicon solar cells via phase separated disordered nanopillars," Nanoscale **10**, 6651–6659 (2018).
68. Y. Zhang, Y. Xu, S. Chen, H. Lu, K. Chen, Y. Cao, A. E. Miroshnichenko, M. Gu, and X. Li, "Ultra-broadband directional scattering by colloidally lithographed high-index Mie resonant oligomers and their energy-harvesting applications," ACS Appl. Mater. Interfaces **10**, 16776–16782 (2018).
69. V. A. Markel and A. K. Sarychev, "Propagation of surface plasmons in ordered and disordered chains of metal nanospheres," Phys. Rev. B **75**, 085426 (2007).
70. F. Rüting, "Plasmons in disordered nanoparticle chains: localization and transport," Phys. Rev. B **83**, 115447 (2011).
71. S. V. Karpov, I. L. Isaev, A. P. Gavrilyuk, V. S. Gerasimov, and A. S. Grachev, "Defects of colloidal crystals," Colloid J. **71**, 329–339 (2009).
72. S. V. Karpov, I. L. Isaev, V. S. Gerasimov, and A. S. Grachev, "Effect of defects of plasmon resonance colloidal crystals on their extinction spectra," Opt. Spectrosc. **109**, 372–378 (2010).
73. P. Moitra, B. A. Slovick, Z. Gang Yu, S. Krishnamurthy, and J. Valentine, "Experimental demonstration of a broadband all-dielectric metamaterial perfect reflector," Appl. Phys. Lett. **104**, 171102 (2014).
74. T. J. Arruda, A. S. Martinez, and F. A. Pinheiro, "Controlling optical memory effects in disordered media with coated metamaterials," Phys. Rev. A **98**, 043855 (2018).
75. M. Yannai, E. Maguid, A. Faerman, Q. Li, J.-H. Song, V. Kleiner, M. L. Brongersma, and E. Hasman, "Order and disorder embedded in a spectrally interleaved metasurface," ACS Photon. **5**, 4764–4768 (2018).
76. A. Rahimzadegan, D. Arslan, R. N. S. Suryadharma, S. Fasold, M. Falkner, T. Pertsch, I. Staude, and C. Rockstuhl, "Disorder-induced

phase transitions in the transmission of dielectric metasurfaces," Phys. Rev. Lett. **122**, 015702 (2019).
77. T. Huang, B. Wang, and C. Zhao, "Negative refraction in metamaterials based on dielectric spherical particles," J. Quant. Spectrosc. Radiat. Transfer **214**, 82–93 (2018).
78. A. E. Ershov, I. L. Isaev, P. N. Semina, V. A. Markel, and S. V. Karpov, "Effects of size polydispersity on the extinction spectra of colloidal nanoparticle aggregates," Phys. Rev. B **85**, 1–10 (2012).
79. G. W. Mulholland, C. F. Bohren, and K. A. Fuller, "Light scattering by agglomerates: coupled electric and magnetic dipole method," Langmuir **10**, 2533–2546 (1994).
80. O. Merchiers, F. Moreno, F. González, and J. M. Saiz, "Light scattering by an ensemble of interacting dipolar particles with both electric and magnetic polarizabilities," Phys. Rev. A **76**, 1–12 (2007).
81. C. F. Bohren and D. R. Huffman, *Absorption and Scattering of Light by Small Particles* (Wiley-VCH, 1998).
82. V. E. Babicheva and A. B. Evlyukhin, "Resonant lattice Kerker effect in metasurfaces with electric and magnetic optical responses," Laser Photon. Rev. **11**, 1700132 (2017).
83. A. García-Etxarri, R. Gómez-Medina, L. S. Froufe-Pérez, C. López, L. Chantada, F. Scheffold, J. Aizpurua, M. Nieto-Vesperinas, and J. J. Sáenz, "Strong magnetic response of submicron silicon particles in the infrared," Opt. Express **19**, 4815–4826 (2011).
84. D. Smirnova, A. I. Smirnov, and Y. S. Kivshar, "Multipolar second-harmonic generation by Mie-resonant dielectric nanoparticles," Phys. Rev. A **97**, 013807 (2018).
85. C. Zhang, Y. Xu, J. Liu, J. Li, J. Xiang, H. Li, J. Li, Q. Dai, S. Lan, and A. E. Miroshnichenko, "Lighting up silicon nanoparticles with Mie resonances," Nat. Commun. **9**, 2964 (2018).
86. P. D. Terekhov, K. V. Baryshnikova, Y. A. Artemyev, A. Karabchevsky, A. S. Shalin, and A. B. Evlyukhin, "Multipolar response of nonspherical silicon nanoparticles in the visible and near-infrared spectral ranges," Phys. Rev. B **96**, 035443 (2017).
87. E. D. Palik, *Handbook of Optical Constants of Solids II* (Academic, 1998).
88. J. R. Allardice and E. C. Le Ru, "Convergence of Mie theory series: criteria for far-field and near-field properties," Appl. Opt. **53**, 7224–7229 (2014).
89. S. Rodriguez, M. Schaafsma, A. Berrier, and J. Gómez Rivas, "Collective resonances in plasmonic crystals: size matters," Phys. B **407**, 4081–4085 (2012).
90. L. Zundel and A. Manjavacas, "Finite-size effects on periodic arrays of nanostructures," J. Phys. **1**, 015004 (2019).
91. D. G. Baranov, D. A. Zuev, S. I. Lepeshov, O. V. Kotov, A. E. Krasnok, A. B. Evlyukhin, and B. N. Chichkov, "All-dielectric nanophotonics: the quest for better materials and fabrication techniques," Optica **4**, 814–825 (2017).